Particuology xxx (xxxx) xxx

Contents lists available at ScienceDirect

Particuology

journal homepage: www.elsevier.com/locate/partic

Measuring permeability and flowability of powders at various packing fractions

Marco Lupo [a, *], Aurélien Neveu [a], Thomas Gemine [a, b], Filip Francqui [a], Geoffroy Lumay [b]

[a] Granutools, Rue Jean-Lambert Defrêne, 107, 4340, Awans, Belgium
[b] GRASP Laboratory, CESAM Research Unit, University of Liège, Allée du 6 Août, 19 (B5a, Office 3/53) B-4000 Sart Tilman, Belgium

ARTICLE INFO

Article history:
Received 1 December 2023
Received in revised form
7 March 2024
Accepted 27 March 2024

Handling Editor: Lifang Wu

Keywords:
Permeability
Packing fraction
Low consolidation
Flowability
Tapped density

ABSTRACT

Permeability is a key powder property for many industrial applications as it affects the flowability during powder handling and the quality of the final product. Indeed, the ability of air to pass through a powder bed, quantified by permeability, is decisive for die or bag filling, dry powder inhalers, silo discharge, pneumatic transport, fluidized bed, etc. Usually, the permeability is measured on a powder bed subjected to high consolidation stresses and without the possibility to control the packing fraction of the powder. In the present study, we show how GranuPack measurement can be combined with a permeability measurement cell to measure the permeability at low consolidation and for various packing fractions, which correspond to many process conditions. A selection of usual powders (pharmaceutical excipients and abrasives) has been tested and the results highlight how the permeability can be used to obtain additional information about powder behavior. For that, a two levels analysis is proposed: an entry-level based on straightforward parameters like initial and final (after the tapping process) permeability and a more advanced level based on two new metrics. These metrics are the permeability ratio and the rate of variation of permeability. These parameters are directly related to the powder cohesiveness and hence can be used to complement the classical flowability indexes.

1. Introduction

Powders are widely used in many industrial applications, such as pharmaceutical, additive manufacturing, food, cosmetics manufacturing, metallurgic, and many other processes. Various properties affect powder behavior during manufacturing processes: particle size distribution, particle shape, inter-particular cohesive forces (van der Waals, electrostatic, capillary), interlocking, and friction between the particles. The permeability, defined as the capacity of a material to transmit a fluid, usually air, through its bulk (Zhao et al., 2021), depends also on these properties and influences the efficiency of many processes, as will be detailed hereafter. Therefore, measuring the permeability of a powder is important to understand its behavior in the processes, to improve the process efficiency, and to have better control of the quality of the final product.

During the die-filling step in tablet manufacturing processes, the interaction between the air and the particles determines the extent of the powder aeration, which in turn affects the flowability of the powder during its displacement before entering the die. In addition, the air must go out of the die through the powder to allow a larger densification of the powder in the die. As a result, the permeability determines the weight uniformity, the packing fraction, and the tensile strength of the tablet. All these tablet characteristics, in turn, determine the quality of the final tablet in terms of disintegration and dissolution behavior of the tablet (Van Snick et al., 2017). Zakhvatayeva et al. (Zakhvatayeva et al., 2018) showed that the critical velocity, that is the shoe velocity above which incomplete filling occurs for a single pass over the die (Schneider et al., 2007), is influenced by the powder permeability. In another filling process, capsule filling, permeability also affects the filling weight in dosator nozzle machines. Faulhammer et al. (Faulhammer et al., 2014) showed that powders with low permeability led to higher fill weight compared to high permeability

* Corresponding author.
E-mail addresses: marco.lupo@granutools.com (M. Lupo), aurelien.neveu@granutools.com (A. Neveu), thomas.gemine@uliege.be (T. Gemine), filip.francqui@granutools.com (F. Francqui), geoffroy.lumay@uliege.be (G. Lumay).

https://doi.org/10.1016/j.partic.2024.03.008

Nomenclature

A	Internal cross-section area of the permeability cell, m^2
C_{KC}	Kozeny-Carman parameter, m^2
d_{10}	Particle diameter corresponding to the 10th percentile of the cumulative particle size distribution, m
d_{50}	Particle diameter corresponding to the 50th percentile of the cumulative particle size distribution, m
d_{90}	Particle diameter corresponding to the 90th percentile of the cumulative particle size distribution, m
H	Height of the powder bed, m
k	Permeability, m^2
k_n	Permeability at n, m^2
k_0	Permeability at $n = 0$, m^2
k_{500}	Permeability at $n = 500$, m^2
k_0/k_{500}	Permeability ratio
n	Number of taps
$P_{atm,abs}$	Absolute atmospheric pressure, Pa
P_{powder}	Pressure drop across the powder bed, Pa
P_{powder}/Q	Slope of the inferred pressure curve attributable only to the powder, Pa m^{-3} s
P_{ref}	Pressure drop due to the measurement cell, Pa
P_{ref}/Q_{ref}	Slope of the pressure curve obtained during the measurement of the pressure drop induced by the measurement cell, Pa m^{-3} s
P_{tot}	Gauge pressure, Pa
P_{tot}/Q_{tot}	Slope of the pressure curve obtained during the measurement of the pressure drop induced by the powder and the measurement cell, Pa m^{-3} s
$P_{tot,abs}$	Absolute pressure at the bottom of the cell, Pa
Q	Volumetric flow rate, m^3 s^{-1}

Greek symbols

η	Packing fraction
η_0	Packing fraction at $n = 0$
η_{500}	Packing fraction at $n = 500$
$\sigma\ \eta_0$	The standard deviation of packing fraction at $n = 0$
$\sigma\ \eta_{500}$	The standard deviation of packing fraction at $n = 500$
μ	Dynamic viscosity of air, kg m^{-1} s^{-1}
ρ	Bulk density, kg m^{-3}
ρ_T	True density, kg m^{-3}

Abbreviations

HR	Hausner ratio
P	Pharmatose®
RoV_k	Rate of variation of permeability, m^2
SC	Silicon carbide
ST	SuperTab®

powders. In fact, more cohesive powders with a lower permeability displayed more significant volume reduction during pre-compaction allowing for higher fill weights compared to powders with larger particles and higher permeability.

In dry powder inhalers (DPI), permeability affects the effective dispersion and release of an inhalation mixture. It must be not too high to improve the dispersion forces within dry powder inhalers during aerosolization but not too low in order not to reduce the DPI performance (Shalash et al., 2018). Hertel et al. (Hertel et al., 2018) were able to find the optimal amount of lactose fines needed in dry powder inhalers to improve the dispersion performance by measuring the permeability of different mixtures.

During powder silo discharges, the air needs to easily permeate the powder to allow it to get out from the silo more easily. Compared to coarse particles, when finer particles are discharged from the silo, the air flows with difficulty through the powder because of much lower permeability, leading to an erratic powder flow, reduced discharge rate, and less steady flow. On the contrary, during the discharge of coarse particles, the air flows upwards through voids between the grains without significant disturbance to the particle flow (Hsiau et al., 2012).

In additive manufacturing processes, it is needed to create dense and homogenous powder layers to improve the quality of the final part. Permeability plays an important role since low permeability causes air to be retained in the powder bulk, limiting the densification of the powder and leading to poor layer uniformity. In addition, the permeability influences the powder spreadability (Davies et al., 2022).

Permeability has been already investigated for powders subjected to normal consolidation stresses. Zhao et al. (Zhao et al., 2021) studied the effect of vibration on the permeability of hard and soft wheat flours subjected to normal stresses between 3 and 9 kPa. Other research works were focused on powders used for DPI formulations (Eike & Steckel, 2012; Zellnitz et al., 2021), wheat flours (Bian et al., 2015), and pharmaceutical excipients (Zakhvatayeva et al., 2018) where the permeability has been measured by applying consolidation stresses up to 15−30 kPa. But, in the applications listed heretofore (die or capsule filling, recoating process) the powder experiences low consolidation stresses or reaches low packing conditions. In these cases, it is important to measure the permeability at low consolidation conditions to properly analyze the powder behavior in the same conditions as in the process. Moreover, during the process, the packing fraction can vary because of the movements induced to the powder by the process itself. Therefore, it is also needed to study the effect of variation of packing fraction on the permeability.

In this paper, we propose a new method combining an automatized tapped density measurement and a permeability measurement. Practically, the GranuPack (from Granutools, Belgium) instrument is equipped with a permeability measurement cell. The first one allows to induce taps to increase the packing fraction of the powder without any applied consolidation stress. The second one allows to measure the permeability at different packing fractions. A set of common pharmaceutical excipients and abrasives have been tested with the measurement device. The excipients are characterized by different particle shapes and sizes, while the abrasives are characterized by the same particle shape but different particle sizes. The effect of packing fraction on permeability and the link with the flowability are analyzed.

2. Material and methods

2.1. Methods

The GranuPack instrument (Granutools, Belgium), which is an automated tapped density tester (Lumay et al., 2012; Traina et al., 2013), has been equipped with a measurement cell to measure the powder permeability at different packing fractions. As shown in Fig. 1, the cell presents a porous material at the bottom to prevent the powder from entering the air supply pipe but allow the passage

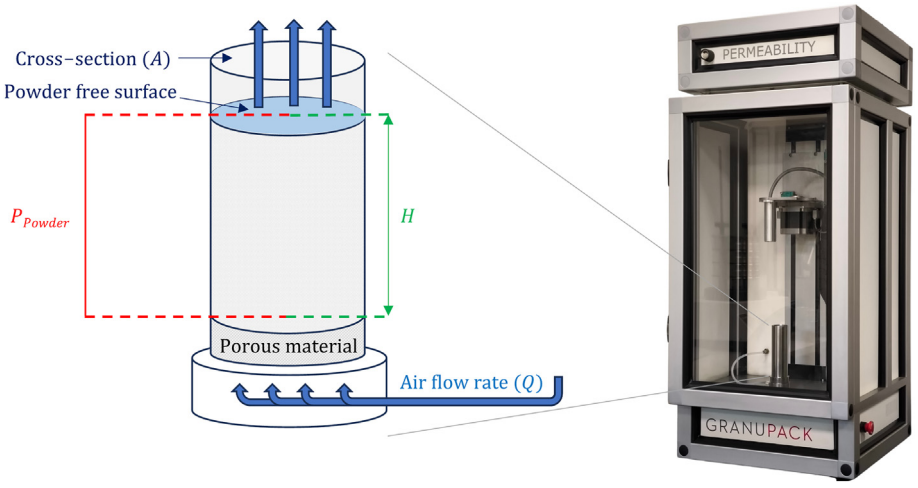

Fig. 1. Sketch of the cell used for powder permeability measurement. At the bottom, the cell presents a porous material to allow the air, fed by the pump, to pass through the powder sample. The pressure drop across the powder bed (P_{powder}) and the insufflated air flow rate (Q) are measured with a pressure and a flow sensor, respectively.

of the air. A dedicated airflow controller injects dry air through the measurement cell at a controlled volumetric air flow rate Q (expressed in m^3/s) and measures the gauge pressure P_{tot} at the bottom of the cell. This gauge pressure is the difference between the absolute pressure at the bottom of the cell $P_{tot,abs}$ and the absolute atmospheric pressure $P_{atm,abs}$. Therefore, the gauge pressure P_{tot} corresponds to the pressure drop due to both the powder bed P_{powder} and the measurement cell (the porous material, tubes, and connections) P_{ref}. Therefore, $P_{tot} = P_{powder} + P_{ref}$. For the sake of simplicity, we will refer to these quantities as pressure instead of pressure drop or gauge pressure in the rest of the paper.

When a powder is submitted to an air flow, two main regimes are observed as a function of the flow rate: the "fixed bed" regime and the "fluidized bed" regime (Seville, 2007). In the first regime, particles are stationary and the gas flows through the interstices. When the bed expands, the bed passes from the fixed to the fluidized bed regime (Bi, 2020). The latter is complex with a wide variety of sub-regimes including homogeneous bed, bubbling, slugging, and turbulent behaviors. Fig. 2 presents a typical pressure curve showing the pressure P_{tot} as a function of the flow rate Q for a typical powder. This curve is obtained by increasing slowly the flow rate Q starting from zero and measuring the corresponding pressure P_{tot}. The pressure evolves linearly in the fixed bed regime and saturates in the fluidized regime. Fitting the linear regime with a least square regression equation gives the slope P_{tot}/Q. We focus on the fixed bed regime allowing to use Darcy's law relating the flow rate and the pressure drop through the permeability in porous materials. In particular, the permeability expressed in square meters is computed with the relation:

$$k = \frac{\mu H}{A}\frac{Q}{P_{powder}} \tag{1}$$

where μ is the dynamic viscosity of air (1.85×10^{-5} kg m^{-1} s^{-1} at 25 °C and 1 atm), H is the height of the powder bed, A is the internal cross-section area of the cell.

The steps carried out to measure the permeability are the following:

1) Evaluation of the pressure drop induced by the measurement cell (P_{ref}). A pressure curve is measured with the empty cell (i.e. without powder) and the slope P_{ref}/Q_{ref} is computed. Measuring the slope of the pressure curve is much more accurate than measuring a single pressure and the corresponding flow rate.
2) The airflow is switched off.
3) The powder is poured into the cell using the GranuPack initialization protocol.
4) Measurement of the initial permeability k_0. A pressure curve is recorded to compute the slope P_{tot}/Q_{tot}. It is important to stay in the linear regime corresponding to the fixed bed to avoid fluidization and therefore a modification of the packing fraction. Looking at the shape of the pressure curve allows us to check that we are in the linear regime. The contribution of the cell is deduced and thus the slope is computed as $P_{powder}/Q = P_{tot}/Q_{tot} - P_{ref}/Q_{ref}$. Then, the permeability is computed using Eq. (1). By doing so, we measure the powder's permeability by subtracting the cell's contribution to the total permeability.
5) The airflow is switched off.
6) A light hollow cylinder called "diabolo" is placed on top of the powder bed and the packing procedure is started. A predefined number of taps (n) is applied to the powder and the bulk density is measured.
7) The "diabolo" is gently removed.

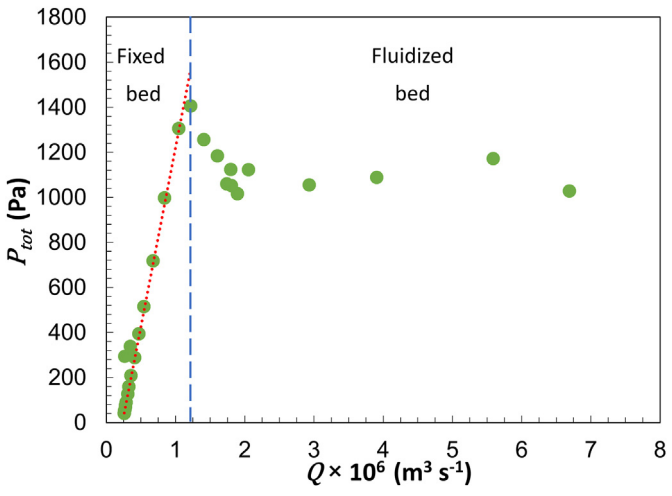

Fig. 2. Typical pressure curve showing the total gauge pressure as a function of the airflow rate Q for ST21AN: the red dotted line is the linear fit, and the blue hyphenated line divides the fixed bed region from the fluidized bed region.

8) The permeability after n taps (k_n) is measured with the same method as described in step 4).
9) The steps 6) to 8) can be repeated.

Independently of the permeability measurement, the GranuPack provides the packing curve, that is the bulk density of the powder as a function of the number of taps, the Hausner ratio (HR), which is the ratio between the final and initial bulk density, and is commonly used to predict the powder flowability in quasi-static conditions, and other information on powder flowability and packing dynamics (Lumay et al., 2020). The results can be expressed in terms of densities ρ or packing fraction η. The packing fraction η is computed from the density ρ and the true density ρ_T with the relation $\eta = \rho/\rho_T$.

Combined with the permeability cell, the GranuPack instrument is highly versatile allowing to define many different measurement protocols and sequences. In this paper, we show data sets with permeability measurements performed for different tap numbers, allowing to perform a deep analysis. However, for a fast and efficient powder characterization, we recommend two permeability measurements: an initial one just after the powder bed formation (k_0) and a final one (k_{500}) after the whole tapping process. But of course, as shown hereafter, additional intermediate permeability measurements can be performed to go deeper in the analysis.

2.2. Materials

The excipients are lactose powders from DFE Pharma (Goch, Germany): Pharmatose® (P) grades 150M, 200M, 450M, and SuperTab® (ST) grades 11SD, 21AN, 24AN, 30GR. These powders differ in shape (see Fig. 3) and size (see Table 1). In Table 1, the powders are reported in order of decreasing particle diameter corresponding to the 50th percentile of the cumulative particle size (d_{50}). The material properties reported in Table 1 are commercial information provided by the producer. Pharmatose grades and ST21AN are composed of irregularly shaped particles, while ST11SD is composed of almost spherical particles. The particles of ST24AN and ST30GR are irregular but with rounded edges. Globally, Pharmatose grades present smaller particle sizes compared to the SuperTab ones.

Table 1
Material properties of lactose powders: ρ_T is the true density, d_{10}, d_{50}, and d_{90} are the particle diameters corresponding to the 10th, 50th, and 90th percentile of the cumulative particle size distribution, respectively, and the span.

Powder	ρ_T (g/cm^3)	d_{10} (μm)	d_{50} (μm)	d_{90} (μm)	Span
ST21AN	1.5815	24.05	179.69	386.64	2.02
ST30GR	1.53225	38.32	126.39	297.3	2.05
ST24AN	1.5404	36.99	121.43	298.04	2.15
ST11SD	1.5363	44	118.7	223.33	1.51
P150M	1.53475	7.37	68.35	189.34	2.66
P200M	1.5366	4.37	37.73	111.33	2.83
P450M	1.53665	3.01	18.27	49.44	2.54

The abrasive powders from EXTROM® (Liège, Belgium) are composed of silicon carbides (SC), which present almost the same irregular shape (see Fig. 4) but different average particle sizes. In the following, the word SC followed by a number refers to Silicon Carbide powder with a specific average particle size. For example, SC5 means the Silicon Carbide powder with an average particle size of 5 mm. The true density of the silicon carbide is $\rho_T = 3.175$ g/cm^3. The material data (particle size and true density) have been taken from the producer documentation.

3. Results and discussion

3.1. Packing dynamics and flowability

Before focusing on permeability, the packing dynamics, and the corresponding flowability indexes are analyzed. Fig. 5 shows the packing curves for the lactose and abrasive powders. Each curve corresponds to an average over a repetition of three measurements and the error bars correspond to the standard deviation. Globally, the powders are well differentiated, as demonstrated by a clear distinction between the packing curves. The data extracted from these packing curves are presented in Table 2. Looking separately at the lactose and the abrasive powders, the *HR* increases when the grain size decreases (Table 1), and/or the particle shape passes from being more spherical to more irregular (Fig. 3). This result makes sense since the lower the grain size and the more irregular the particle shape, the larger the interparticle cohesive forces

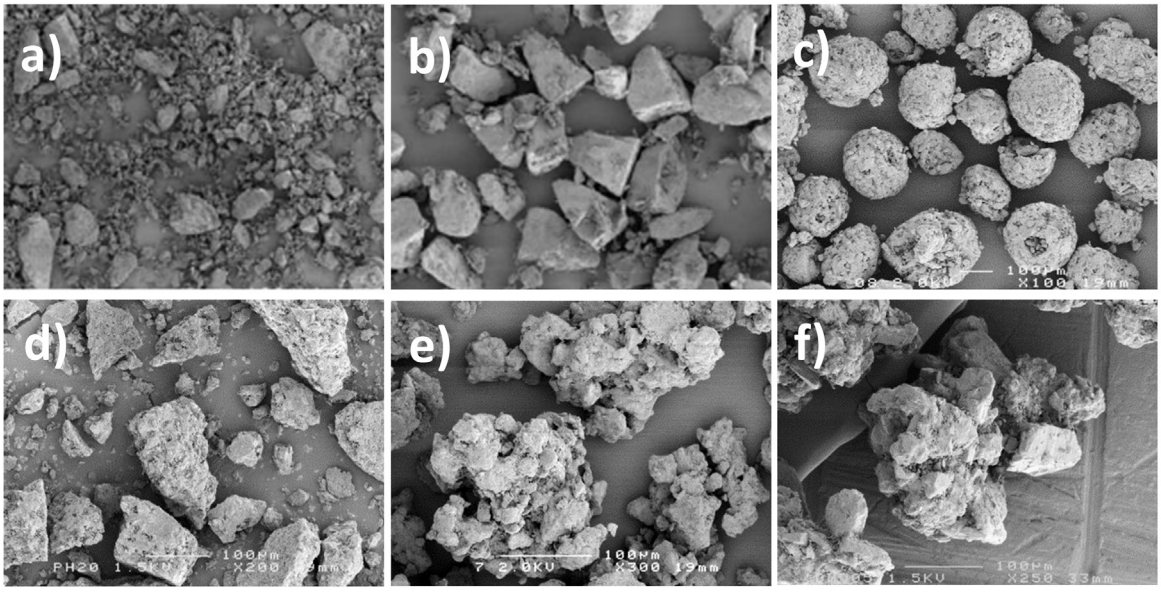

Fig. 3. SEM images of: (a) P450M and P200M, (b) P150M, (c) ST11SD, (d) ST21AN, (e) ST24AN, (f) ST30GR. These images were provided by the DFE Pharma (Goch, Germany).

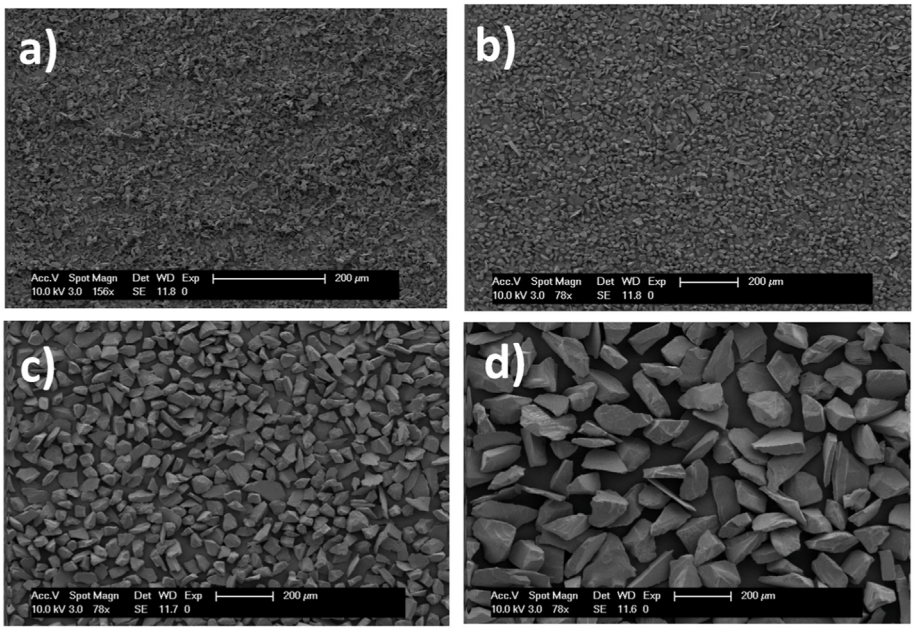

Fig. 4. Selection of SEM images of silicon carbide powders: (a) SC13, (b) SC23, (c) SC50, (d) SC100.

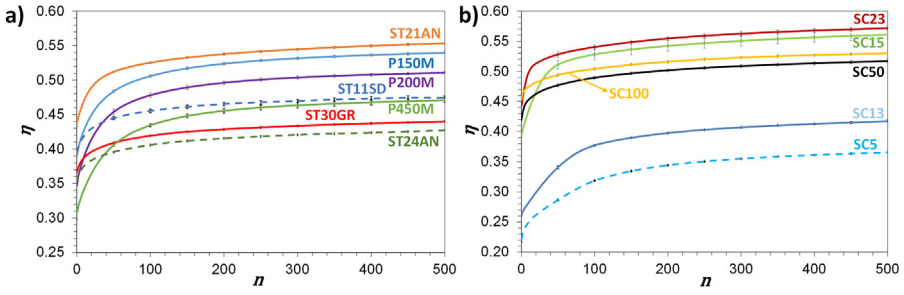

Fig. 5. Packing curves for (a) lactose and (b) abrasive powders.

Table 2
Initial (η_0), final (η_{500}) packing fractions with the standard deviations among three measurements ($\sigma\ \eta_0$ and $\sigma\ \eta_{500}$) and Hausner ratio (*HR*) for lactose and abrasive powders.

Name	η_0	$\sigma\ \eta_0$	η_{500}	$\sigma\ \eta_{500}$	*HR*
P450M	0.307	0.009	0.471	0.004	1.54
P200M	0.347	0.009	0.511	0.002	1.47
P150M	0.392	0.004	0.540	0.002	1.38
ST21AN	0.437	0.003	0.553	0.001	1.27
ST24AN	0.353	0.004	0.427	0.001	1.21
ST11SD	0.395	0.004	0.475	0.002	1.20
ST30GR	0.366	0.004	0.440	0.001	1.20
SC5	0.222	0.005	0.366	0.001	1.65
SC13	0.262	0.000	0.418	0.002	1.59
SC15	0.394	0.002	0.561	0.008	1.42
SC23	0.443	0.003	0.572	0.003	1.29
SC50	0.419	0.002	0.517	0.003	1.23
SC100	0.452	0.003	0.530	0.001	1.17

compared to the grain weight, and consequently the lower the powder flowability.

In the case of the lactose powders (Table 2) based on the ranges of *HR* values (Kalman, 2021), it is possible to distinguish three groups of powders: one composed of ST30GR, ST11D, and ST24AN, one composed of ST21AN and P150M, and the last one composed of P200M and P450M. Powders of the first group present the smallest increase in the packing fraction as demonstrated by the lowest *HR* value, below 1.22, which denotes a fair flowability behavior. The second group presents powders with intermediate *HR* values, between 1.27 and 1.38, which indicates passable or poor flowability behavior. The last group is composed of powders with an *HR* greater than 1.46, which corresponds to very poor flowability behavior. The ST21AN presents the smallest *HR* values among the less flowable powders (*HR* above 1.25). This result could be explained by the fact that ST21AN presents larger particles compared to the Pharmatose powders. Therefore, its behavior is in between that of the Pharmatose powders, which present both irregular and small particles, and the SuperTab powders, which present big and regularly shaped particles.

The abrasive powders can be differentiated according to the *HR* values as follows (Table 2): SC100 and SC50 present an *HR* below 1.24, which denotes a good flowability behavior; SC23 and SC15, present an *HR* between 1.29 and 1.42, which indicates a passable/poor flowability behavior; SC13 and SC5, which present an *HR* above 1.58, which indicates a very poor flowability behavior. These powders have similar particle shapes, therefore the factor that determines the different flowability behavior is the particle size. Indeed, as the particle size decreases, the *HR* increases accordingly.

3.2. Permeability versus packing fraction

Following the measurement procedure described in section 2.1, the influence of the packing fraction η on the permeability k has been analyzed for the whole set of powders. More precisely, the permeability and the packing fraction have been measured for a sequence of tap numbers. The corresponding trends are reported in Fig. 6. All the powders (lactose and abrasive) show a decrease in the permeability with packing fraction. This result makes sense since the higher the powder densification under the tapping process, the closer the particles and consequently the lower the space available for the air to pass through the particles, which means a lower permeability compared to the initial condition. However, the curves do not follow a master curve showing that the packing fraction is not the only parameter influencing the permeability. Indeed, the particle size distribution and shape influence the geometry and the distribution of the pores, modifying the permeability.

In Fig. 6, error bars are reported for the first and last measurement of each set and are based on three repetitions. The initial point (lower packing fraction) is characterized by larger error bars compared to the last point (higher packing fraction). The larger variation of the measurement for initial permeability can be explained by the larger variability in the particle arrangement in loose conditions compared to a more uniform and controlled particle arrangement after tapping.

Fig. 6 also shows that, depending on the packing fraction value, the permeability can change significantly. This is, for example, the case of the SC100, for which small variations in the packing fraction induce a large variation in the permeability. Therefore, it is important to measure the permeability in the same packing conditions of the process to avoid wrong estimations and to properly compare different powders.

3.3. Permeability versus flowability

Measuring a whole set of permeabilities for different tap numbers and their corresponding packing fractions is interesting for a deep analysis but also time-consuming. In this section, we show that interesting powder characterization information can be found by focusing only on the initial (0 taps) and final (500 taps) values of the parameters. Fig. 7 shows the initial k_0 and final k_{500} permeabilities and the corresponding packing fraction values (η_0 and η_{500}) as a function of the *HR* for lactose powders.

Concerning the initial permeability k_0, two regimes are observed: a decrease of the permeability followed by an increase (see Fig. 7). The points at low *HR* correspond to lactose powders (ST11SD, ST24AN, and ST30GR) with the larger grains having therefore a low cohesiveness. The higher permeability is explained by a distribution of larger voids between the larger grains. Instead, above $HR = 1.25$, permeability increases with HR. This increase can be explained by the decrease of the packing fraction with the increase of the powder cohesiveness. Indeed, the cohesive forces can stabilize a loose packing having a high porosity. Consequently, the larger the powder cohesiveness, the less dense the powder bed and the larger the permeability. This effect is clearly shown in the case of ST21AN, P150M, P200M, and P450M, which are composed of small and/or irregularly shaped particles and hence more cohesive compared to the other powders.

After 500 taps, permeability decreases for all the powders because of the increase in the packing fraction (see Fig. 7(b)). This result can be explained by the higher densification of the cohesive powders, represented by larger *HR* values, compared to more flowable powders. The larger the powder cohesiveness, the larger the powder densification by tapping, and the lower the permeability.

Fig. 8 shows k_0, k_{500}, η_0, and η_{500} as a function of the *HR* for the abrasive powders. The behavior is qualitatively similar to lactose powders, with a higher initial permeability for both larger grains and low *HR* and smaller cohesive grains at higher *HR*. In between a minimum of the permeability is measured. The final permeability k_{500} decreases with *HR*. These dependencies are only related to grain size since the different abrasives are composed of irregular particles of similar shape.

One significant result emerging from the results obtained on both the lactose (Fig. 7) and the abrasive powders (Fig. 8) is that the final permeability (measured after 500 taps) can be used to predict the powder flowability: the lower the *HR* the larger the permeability.

3.3.1. Permeability ratio

Similarly to the *HR*, which is used to classify the powders based on the increase of the bulk density with the applied taps, a new parameter is proposed to differentiate the powders based on their capacity to decrease the permeability with the increase of the packing fraction because of taps. This parameter is the permeability ratio, k_0/k_{500}, which is the ratio between the initial and the final permeability. Similarly to the *HR*, the ratio k_0/k_{500} is greater than unity.

Fig. 9 shows the permeability ratio (k_0/k_{500}) as a function of the *HR* for the lactose powders. The larger the increase in the packing fraction of the powder, that is the larger the *HR*, the larger the reduction in powder permeability between $n = 0$ and $n = 500$. This result could be explained by the fact that the more cohesive the powder, the larger the increase in the packing fraction, and hence the larger the variation in the powder configuration because of taps compared to a more flowable powder, and the larger the effect on the variation in permeability.

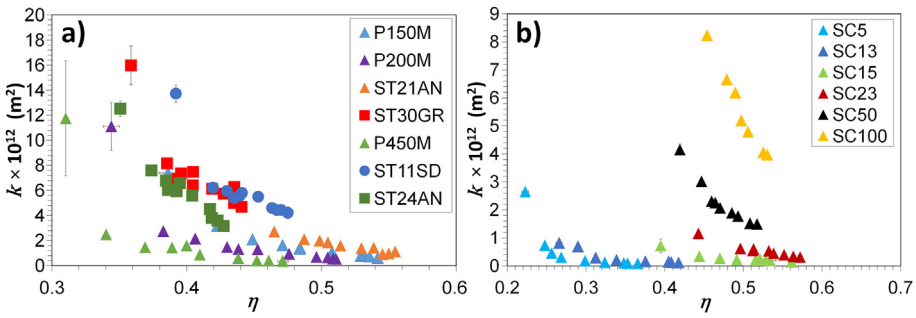

Fig. 6. Evolution of permeability k with the packing fraction η for (a) lactose powders and (b) abrasive powders. The error bars are reported only for the first and last measurement of each set and are based on three repetitions.

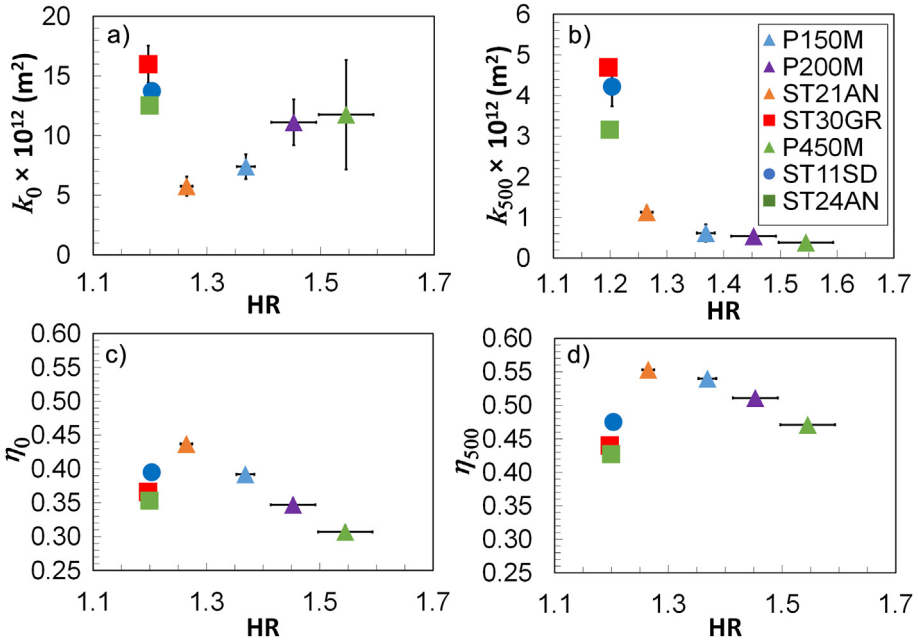

Fig. 7. (a) Initial permeability k_0, (b) final permeability k_{500}, (c) initial packing fraction η_0, and (d) final packing fraction η_{500} as a function of the Hausner ratio (*HR*) for the set of lactose powders.

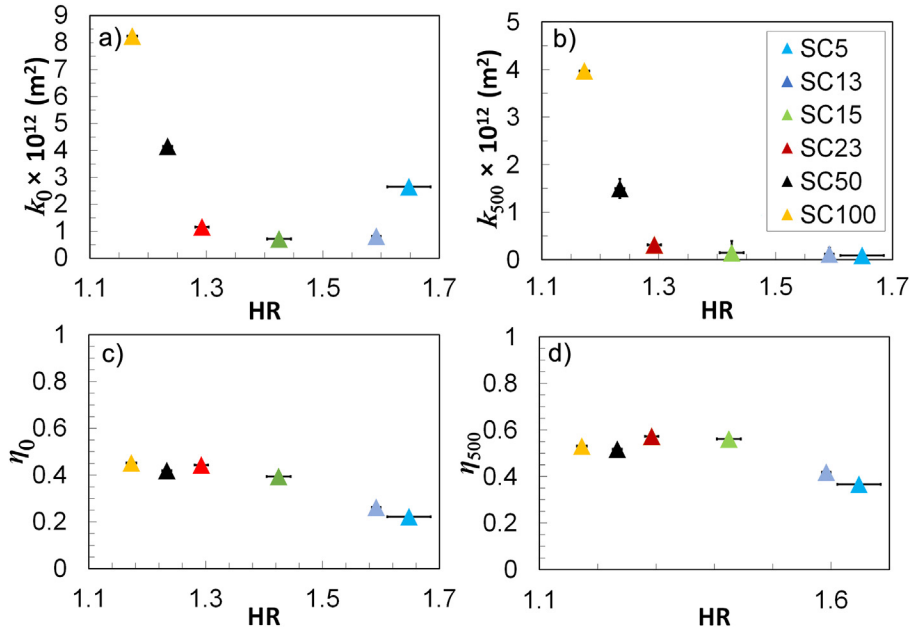

Fig. 8. (a) Initial permeability k_0, (b) final permeability k_{500}, (c) initial packing fraction η_0, and (d) final packing fraction η_{500} as a function of the *HR* for abrasive powders.

The most flowable powders (ST11SD, ST30GR, and ST24AN) experience only a reduced variation of the permeability, i.e. k_0/k_{500} below 5, while the cohesive powders (the Pharmatose grades and ST21AN) experience larger permeability variations.

Similarly to the lactose powders, the abrasive powders present an increase in the permeability ratio with the increase of the powder cohesiveness (Fig. 10). When the *HR* is above 1.42, the permeability ratio increases more significantly with the increase of the *HR*, compared to lower values of the *HR*.

Because of the direct dependency between the k_0/k_{500} and the HR, the permeability ratio could be used to predict the powder flowability.

3.4. Rate of variation of permeability

A second original metric is proposed to classify the powders based on how fast is the variation of the permeability with the applied taps. Looking at the evolution of permeability with the

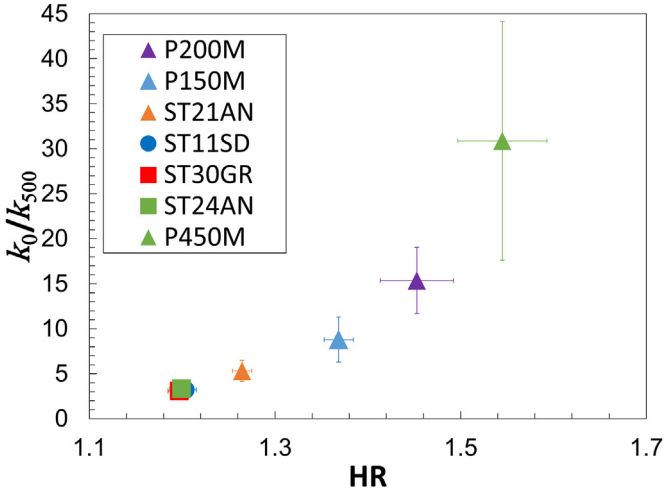

Fig. 9. Permeability ratio (k_0/k_{500}) as a function of the *HR* for lactose powders.

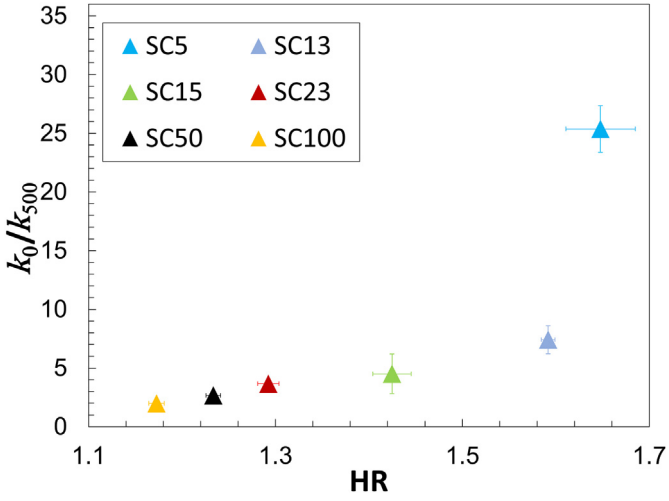

Fig. 10. Permeability ratio (k_0/k_{500}) as a function of the *HR* for abrasive powders.

packing fraction of lactose powders (Fig. 11(a)), it is evident that, except for the first point ($n = 0$) of each set of permeability values, the other points follow a linear trend. It means that as soon as some taps are applied to the powder, the permeability values start to decrease linearly with the increase of the packing fraction. By approximating the data for each powder with a regression line (Fig. 11(a)), by using the method of least squares, the corresponding slope value is the rate of variation of permeability (RoV_k). This parameter quantifies how fast is the decrease of the permeability with the increase of the packing fraction. To distinguish the powders based on the RoV_k, the parameter has been reported as a function of the *HR* in Fig. 11(b).

Looking at the RoV_k as a function of the *HR*, it is observed that the less cohesive the powder (lower *HR*), the larger the parameter in absolute value. This result could be explained by the easier capacity of more flowable powders to rearrange the particles and consequently modify the distribution of the voids, which affects the permeability.

In the case of the abrasives (Fig. 12(a)), for some powders only the final points of the permeability-packing fraction curves follow a linear trend. Therefore, to compare all the powders in terms of the

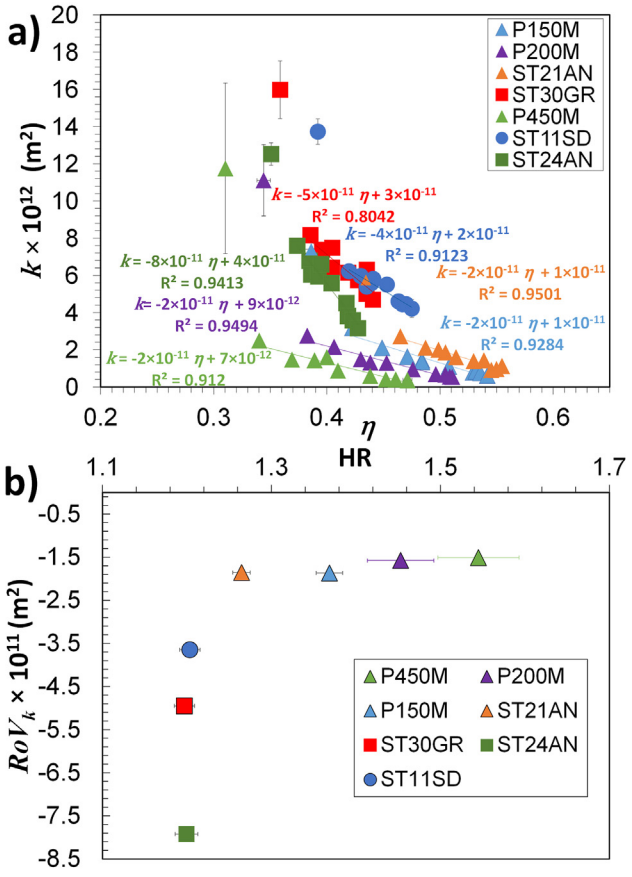

Fig. 11. Lactose powders: (a) Evolution of permeability with the packing fraction, the regression lines, and the corresponding equations, and (b) rate of variation of permeability (RoV_k) as a function of the *HR*.

RoV_k, only the final five data points, that are at the largest packing fraction values, have been considered for the linear regression.

As the lactose powders, the larger the powder flowability the faster the decrease in the permeability with the packing fraction (Fig. 12(b)). It is interesting to note that the RoV_k goes in the opposite direction to the k_0/k_{500}: with the increase of the *HR*, the first one decreases, and the second one increases. It means that the more cohesive the powder, the larger the decrease of the permeability with the densification but the slower this decrease compared to more flowable powders. More cohesive powders are characterized by larger densification because of taps, which leads to larger variation in the particle rearrangement and thus to a larger reduction in permeability. Compared to more flowable powders, in cohesive powders, the particle rearrangement and, consequently, the permeability variation, are more significant but occur more slowly.

Together with the permeability ratio and because of the link between the *HR* and the RoV_k, this latter parameter could be used to complement the classical flowability indexes.

3.5. Application of Kozeny-Carman equation

The Kozeny-Carman equation is a well-known model (Börjesson et al., 2016; Carman, 1937; Kozeny, 1927), which combines the Darcys' law and the Poiseuille equation in a straight channel to obtain a relation between the permeability, the packing fraction, and the characteristics of the powder bed (Costa, 2006). The equation is:

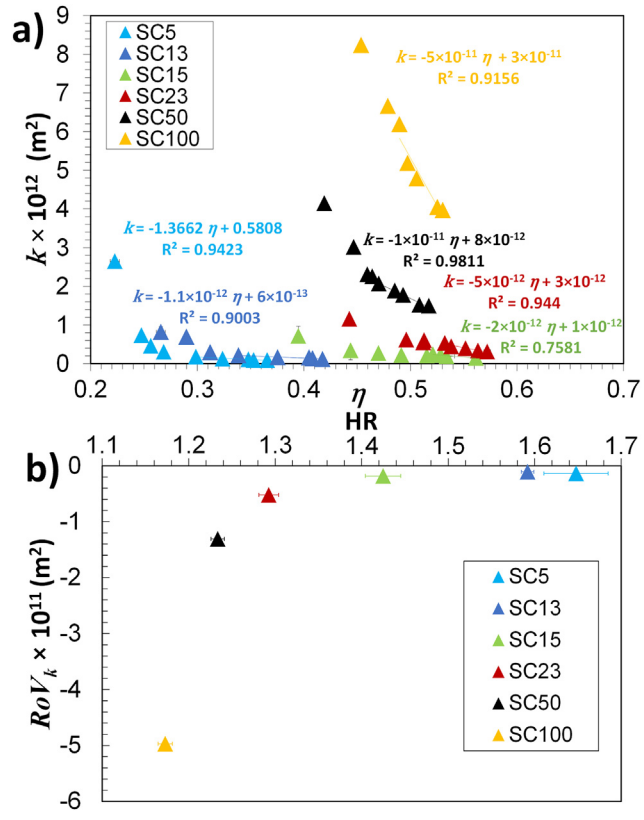

Fig. 12. Abrasive powders: (a) Evolution of permeability with the packing fraction, the regression lines, and the corresponding equations, and (b) rate of variation of permeability (RoV_k) as a function of the *HR*.

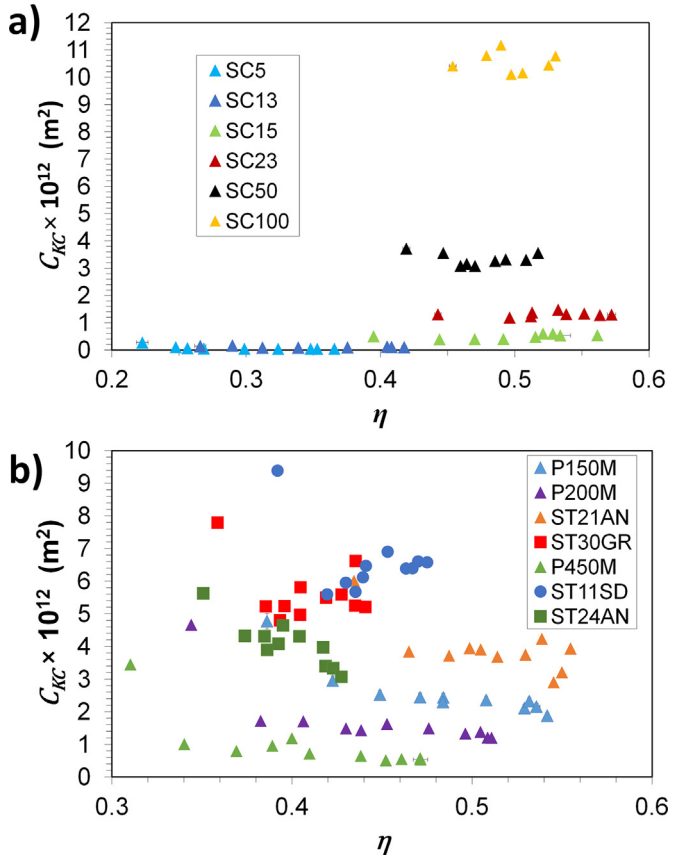

Fig. 13. Kozeny-Carman constant as a function of the packing fraction for the abrasive (a) and the lactose (b) powders.

$$k = C_{KC}\frac{(1-\eta)^3}{\eta^2} \tag{2}$$

where C_{KC} is the Kozeny-Carman parameter. It depends on the assumed shape of the capillaries perforating the porous media, their tortuosity, and the particle structure.

Eq. (2) has been used to get the C_{KC} by using the permeability measured with the permeability cell at different packing fractions. The results are reported in Fig. 13. We observe that C_{KC} remains constant for the abrasives (Fig. 13(a)) while varying the packing fraction, in accordance with the Kozeny-Carman equation prediction. Therefore, the C_{KC} can be directly obtained with the method proposed in this paper.

For the lactose powders (Fig. 13(b)), the C_{KC} is not constant and depends also on the packing fraction. This result indicates that the Kozeny-Carman model cannot be applied to all kinds of materials, as already stressed by Börjesson et al. (Börjesson et al., 2016) in the case of powder beds consisting of spray-dried dairy powders. The good estimation of the C_{KC} for the abrasives, can be explained by the nature of the abrasive powders. In fact, the abrasives used in this study can be considered model powders, having a monodispersed distribution and composed of particles with the same shape.

4. Conclusions

A new procedure for the measurement of the permeability as a function of the packing fraction at low consolidation conditions has been proposed. It combines the capacity of the GranuPack to control the densification of the powder and the possibility of measuring the permeability in correspondence with the obtained packing fraction values by using a purposely developed cell.

Different lactose grades, characterized by different particle shapes and sizes, and abrasive powders, characterized by the same irregularly shaped particle but different particle sizes, have been tested with the GranuPack.

The permeability evolution with the packing fraction has been obtained for all the powders. The results have shown that the larger the packing fraction the lower the permeability and, for some powders, a small modification of the packing fraction can lead to large variations in the permeability. Therefore, it is important to measure the permeability in the same densification condition of the process to correctly understand the effect of permeability on the process, to properly compare the powders, and to properly design the process to maximize the efficiency or improve the product quality.

By comparing the permeability classification at loose and packed conditions, it has been found that the powder classification can change depending on the densification conditions. In particular, at 500 taps, the larger the powder cohesiveness, the lower the permeability. Consequently, the permeability after the densification (500 taps) could be used to predict the powder flowability.

Two new metrics have been proposed to quantify the effect of densification on permeability: the permeability ratio and the rate of variation of permeability. The first one quantifies the reduction of permeability because of taps. The second one defines how fast is the reduction of permeability due to the densification. The results have shown that when the powder cohesiveness increases, the permeability ratio increases, and the rate of variation of

permeability decreases. Therefore, these two parameters could help in predicting powder flowability.

Finally, the proposed method has been applied to determine the Kozeny-Carman parameter. We have shown that the Kozeny-Carman parameter is a constant for the abrasives, considered as a model material, but not for the lactose powder. Therefore, the method presented in this article should allow future development of a more elaborated model to describe the interaction between packing properties and permeability.

Declaration of competing interest

The authors declare that they have no known competing financial interests or personal relationships that could have appeared to influence the work reported in this paper.

References

Bi, X. (2020). Gas fluidization flow regimes. In *Essentials of fluidization technology* (pp. 55–74). wiley. https://doi.org/10.1002/9783527699483.CH4.

Bian, Q., Sittipod, S., Garg, A., & Ambrose, R. P. K. (2015). Bulk flow properties of hard and soft wheat flours. *Journal of Cereal Science, 63*, 88–94. https://doi.org/10.1016/j.jcs.2015.03.010

Börjesson, E., Innings, F., Trägårdh, C., Bergenståhl, B., & Paulsson, M. (2016). Permeability of powder beds formed from spray dried dairy powders in relation to morphology data. *Powder Technology, 298*, 9–20. https://doi.org/10.1016/j.powtec.2016.05.006

Carman, P. (1937). Fluid flow through a granular bed. *Transactions of the Institution of Chemical Engineers, 15*, 150–167.

Costa, A. (2006). Permeability-porosity relationship: A reexamination of the Kozeny-Carman equation based on a fractal pore-space geometry assumption. *Geophysical Research Letters, 33*(2), Article L02318. https://doi.org/10.1029/2005GL025134

Davies, R., Evans, K., & Ghita, O. (2022). Multivariate correlation of Poly-ArylEtherKetone powder properties for additive manufacturing and a method for predicting spreading in polymer powder bed fusion. *Powder Technology, 410*, Article 117871. https://doi.org/10.1016/J.POWTEC.2022.117871

Eike, C., & Steckel, H. (2012). Capabilities and limitations of using powder rheology and permeability to predict dry powder inhaler performance. *European Journal of Pharmaceutics and Biopharmaceutics, 82*(2), 417–423. https://www.sciencedirect.com/science/article/pii/S0939641112002433.

Faulhammer, E., Llusa, M., Radeke, C., Scheibelhofer, O., Lawrence, S., Biserni, S., Calzolari, V., & Khinast, J. G. (2014). The effects of material attributes on capsule fill weight and weight variability in dosator nozzle machines. *International Journal of Pharmaceutics, 471*(1–2), 332–338. https://www.sciencedirect.com/science/article/pii/S0378517314004116.

Hertel, M., Schwarz, E., Kobler, M., Hauptstein, S., Steckel, H., & Scherließ, R. (2018). Powder flow analysis: A simple method to indicate the ideal amount of lactose fines in dry powder inhaler formulations. *International Journal of Pharmaceutics, 535*, 59–67. https://www.sciencedirect.com/science/article/pii/S0378517317310323.

Hsiau, S., Liao, C., & Lee, J. H. (2012). The discharge of fine silica sand in a silo under different ambient air pressures. *Physics of Fluids, 24*(4), Article 043301. https://pubs.aip.org/aip/pof/article/24/4/043301/257578.

Kalman, H. (2021). Quantification of mechanisms governing the angle of repose, angle of tilting, and Hausner ratio to estimate the flowability of particulate materials. *Powder Technology, 382*, 573–593. https://doi.org/10.1016/j.powtec.2021.01.012

Kozeny, J. (1927). Ueber kapillare leitung des wassers im boden. *Sitzungsberichte der Akademie der Wissenschaften Wien, 136*, 271–306.

Lumay, G., Boschini, F., Traina, K., Bontempi, S., Remy, J. C., Cloots, R., & Vandewalle, N. (2012). Measuring the flowing properties of powders and grains. *Powder Technology, 224*, 19–27. https://doi.org/10.1016/j.powtec.2012.02.015

Lumay, G., Francqui, F., Detrembleur, C., & Vandewalle, N. (2020). Influence of temperature on the packing dynamics of polymer powders. *Advanced Powder Technology, 31*(10), 4428–4435. https://doi.org/10.1016/j.apt.2020.09.019

Schneider, L. C. R., Sinka, I. C., & Cocks, A. C. F. (2007). Characterisation of the flow behaviour of pharmaceutical powders using a model die-shoe filling system. *Powder Technology, 173*(1), 59–71. https://doi.org/10.1016/j.powtec.2006.11.015

Seville, J. P. K. (2007). Fluidisation of cohesive particles. *Handbook of Powder Technology, 11*, 1041–1069. https://doi.org/10.1016/S0167-3785(07)80057-1

Shalash, A. O., Khalafallah, N. M., Molokhia, A. M., & Elsayed, M. M. A. (2018). The relationship between the permeability and the performance of carrier-based dry powder inhalation mixtures: New insights and practical guidance. *AAPS PharmSciTech, 19*(2), 912–922. https://doi.org/10.1208/S12249-017-0898-7

Traina, K., Cloots, R., Bontempi, S., Lumay, G., Vandewalle, N., & Boschini, F. (2013). Flow abilities of powders and granular materials evidenced from dynamical tap density measurement. *Powder Technology, 235*, 842–852. https://doi.org/10.1016/j.powtec.2012.11.039

Van Snick, B., Holman, J., Cunningham, C., Kumar, A., Vercruysse, J., De Beer, T., Remon, J. P., & Vervaet, C. (2017). Continuous direct compression as manufacturing platform for sustained release tablets. *International Journal of Pharmaceutics, 519*(1–2), 390–407. https://doi.org/10.1016/j.ijpharm.2017.01.010

Zakhvatayeva, A., Zhong, W., Makroo, H. A., Hare, C., & Wu, C. Y. (2018). An experimental study of die filling of pharmaceutical powders using a rotary die filling system. *International Journal of Pharmaceutics, 553*(1–2), 84–96. https://doi.org/10.1016/j.ijpharm.2018.09.067

Zellnitz, S., Lamešić, D., Stranzinger, S., Pinto, J. T., Planinšek, O., & Paudel, A. (2021). Spherical agglomerates of lactose as potential carriers for inhalation. *European Journal of Pharmaceutics and Biopharmaceutics, 159*, 11–20. https://doi.org/10.1016/j.ejpb.2020.12.015

Zhao, Y., Phalswal, P., Shetty, A., & Kingsly Ambrose, R. P. (2021). Effects of powder vibration and time consolidation on soft and hard wheat flour properties. *KONA Powder and Particle Journal, 38*, 226–234. https://doi.org/10.14356/KONA.2021007